EurJIC
European Journal of Inorganic Chemistry

A Journal of ChemPubSoc Europe

Accepted Article

Title: Mechanistic insights into light-activated catalysis for water oxidation

Authors: Mirco Natali, Francesco Nastasi, Fausto Puntoriero, and Andrea Sartorel

To be cited as: *Eur. J. Inorg. Chem.* 10.1002/ejic.201801236

Link to VoR: http://dx.doi.org/10.1002/ejic.201801236

WILEY-VCH

MINIREVIEW WILEY-VCH

Mechanistic insights into light-activated catalysis for water oxidation

Mirco Natali,*[a] Francesco Nastasi, Fausto Puntoriero,[b] and Andrea Sartorel*[a]

Dedicated to Prof. Franco Scandola for his scientific mentorship

Abstract: The development of catalysts for water oxidation to oxygen has been the subject of intense investigation in the last decade. In parallel to the search for high catalytic performance, many works have focused on the mechanistic analysis of the process. In this perspective, the oxidation of water through light-assisted cycles composed of an electron acceptor (EA), a photosensitizer (PS), and a water oxidation catalyst (WOC) can provide insightful and complementary information with respect to the use of chemical oxidants or to electrochemical techniques. In this microreview, we discuss the mechanistic aspects of the EA/PS/WOC photoactivated cycles, and in particular: (i) the general elementary steps; (ii) the required features and the nature of the PS employed; (iii) the electron transfer processes and kinetics from the WOC to PS^+ (hole scavenging); (iv) the detrimental quenching of the PS by the WOC and the alternative mechanistic routes; (v) the identification of WOC intermediates and, finally, (vi) the transposition of the above processes into a dye-sensitized photoanode embedding a WOC.

1. Introduction

In the last decade, many efforts have been focused towards the catalysis for the oxidation of water to dioxygen (eq. 1), since it is a challenging redox reaction within the context of artificial photosynthesis.[1],[2]

$$2\ H_2O \rightarrow O_2 + 4\ H^+ + 4\ e^- \quad (1)$$
(E^0 = +1.23 V vs Normal Hydrogen Electrode, NHE)

Although oxygen can be considered a useless by-product in artificial photosynthesis, water oxidation provides the reducing equivalents necessary for the synthesis of fuels, typically by reduction of protons to hydrogen[3],[4–6] or by reduction of carbon dioxide to carbon monoxide, formic acid, methanol or methane.[7],[8],[9] Efforts in this field have been focused on the development of new and efficient catalysts,[10,11],[12] but also on the mechanistic investigation for the identification of reaction rates and intermediates involved in breaking and formation of bonds, in particular the most challenging one related to the formation of the oxygen-oxygen bond.[13,14]

The activity of water oxidation catalysts (WOCs) can be investigated by several methods. (i) The employment of chemical oxidants, such as cerium ammonium nitrate $(NH_4)_2Ce(NO_3)_6$ (CAN) or sodium periodate, $NaIO_4$,[15] may allow to determine key performance indicators (KPI) of the WOC such as total turnover number (TON, indicative of the robustness of a catalyst) and turnover frequency (TOF, indicative of the efficiency of a catalyst). From the mechanistic standpoint, the employment of chemical oxidants can be useful to determine the kinetic order in catalyst,[16] and to characterize catalyst intermediates involved in the oxygenic cycle, in particular with ruthenium catalysts.[17],[18],[19],[20,21] Drawbacks of chemical oxidants may arise from the restricted pH window of stability, from their specific interactions with the catalyst, and from the fact that they can actually serve as oxygen source in the catalytic process.[15] (ii) The use of electrochemical techniques[22–25] is a clean route to benchmark the activity of water oxidation catalysts, and to determine KPI such as TON, TOF, overpotential, and faradaic yield. These have the advantage of selecting the desired reaction environment, possibly spanning the entire pH region in the case of aqueous solution, and have been also employed for water oxidation catalysis investigation in non-aqueous media.[26],[27] From the mechanistic perspective, electrochemical tools are exploited to determine the homogeneous or heterogeneous nature of the catalytic process,[28] to assess the role of external agents (such as the buffer concentration),[29],[30] to characterize catalyst intermediates when combined with spectroscopic tools, and to have indication of the nature of the rate determining step through Tafel slope analysis,[31] especially when the catalyst is embedded in an electrode (heterogeneous catalysis). Although some caution should be considered in the view of possible specific effects of the working electrode, electrochemical tools are very useful to assess the oxygenic catalytic process, in the perspective of developing water electrolyzers coupled with photovoltaic modules, that constitute a possible device design in artificial photosynthesis.[32] (iii) Differently from the techniques (i) and (ii) described above that refer to dark processes, exploiting light to activate the WOC can be performed by the use of photogenerated oxidants from a photosensitizer (PS) in the presence of an electron acceptor (EA), Scheme 1, similarly to what occurs in natural photosynthesis. In such cycles, besides the catalyst KPI such as TON and TOF, an important one is the photochemical quantum yield (Φ_{O_2}), defined as the ratio between

[a] Dr. M. Natali
Department of chemical and pharmaceutical sciences
University of Ferrara
Via L. Borsari 46, 44121 Ferrara, Italy.
E-mail: mirco.natali@unife.it
http://docente.unife.it/mirco.natali
[b] Dr. F. Nastasi and Prof. F. Puntoriero
Department of chemical, biological, pharmaceutical and environmental sciences and interuniversity centre for artificial photosynthesis (SOLAR-CHEM)
University of Messina
Via Sperone 31, 98166 Messina (Italy).
[c] Prof. A. Sartorel
Department of chemical sciences
University of Padova
Via Marzolo 1, 35131 Padova (Italy)
E-mail: andrea.sartorel@unipd.it
http://www.chimica.unipd.it/category/ruoli/personale-docente?key=B8C9C339BA22FAB3B2DDE61595CB8D7F

the number of evolved oxygen molecules and the absorbed photons by the system.[33,34] The use of light-activated cycles for mechanistic investigation is the subject of this microreview. In particular, we will report mechanistic analysis of photocatalytic water oxidation cycles employing three-component EA/PS/WOC systems. Recently, such photoactivation strategy has been proposed also for the selective oxygenation of organic substrates aimed at the production of added-value products, a complementary and promising strategy to overcome the hurdle of the 4-electron water oxidation cycle.[35–37]

From left to right: Fausto Puntoriero, Francesco Nastasi, Mirco Natali, Andrea Sartorel during the 43rd International Conference on Coordination Chemistry (ICCC2018) in Sendai (Japan), July 30th - August 4th, 2018.

Mirco Natali is assistant professor at the Department of Chemical and Pharmaceutical Sciences of the University of Ferrara. From the same institution he received his PhD in Chemical Sciences in 2014 working in the group of Prof. Franco Scandola. His research interests embrace several aspects of artificial photosynthesis as well as fundamental studies on photoinduced energy and electron transfer processes.

Francesco Nastasi received his PhD degree from the University of Messina in 2009. Currently, he is lecturer B in Physical Chemistry at the University of Messina. His research activity is essentially focused on supramolecular photochemistry and photophysics, with particular attention to the study of energy and electron-transfer processes in systems for the photochemical conversion of solar energy.

Fausto Puntoriero received his PhD from the University of Messina in 2002, under the supervision of Prof. Sebastiano Campagna. At present he is Associate Professor of Physical Chemistry at the Department CHIBIOFARAM of the University of Messina. His research interests include photochemistry, photophysics, and electrochemistry of supramolecular species and photoinduced energy- and electron-transfer processes.

Andrea Sartorel is associate professor at the department of chemical sciences, University of Padova, in the Nano & Molecular Catalysis group. His research interests deal with biomimetic oxidation catalysis by transition metal complexes, aimed at the development of renewable chemical processes exploiting solar light.

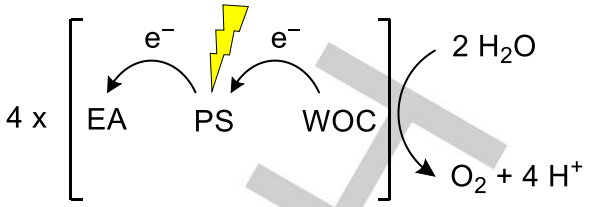

Scheme 1. Photocatalytic water oxidation in an EA / PS / WOC system.

We want to underline that the use of such light-activated cycles by combining the WOC with a PS/EA system can provide additional and complementary information with respect to the use of chemical oxidants or electrochemical tools. Moreover, it should be noticed that in a dye-sensitized photoanode, within a photoelectrochemical cell technology (considered as the most promising one in view of a scalable device for artificial photosynthesis),[32] the actual oxidant is the oxidized form of the dye, generated through a photoactivated process. The review is organized as follows: paragraph 2 includes general mechanistic aspects and the discussion of the photosensitizers employed in such systems, discussing their photophysical and electrochemical properties and related aspects on the photogeneration of the oxidized form PS^+. Paragraph 3 deals with electron transfer rates from the WOC to PS^+ (hole scavenging), a fundamental step in photocatalytic cycles that may impact the efficiency and the stability of the system. In paragraph 4, *PS quenching effects from the WOC and alternative mechanisms are presented. Paragraph 5 reports the characterization of WOC intermediates within the photocatalytic cycle. Finally, paragraph 6 reports conclusions and perspectives related to the transposition of the mechanistic information from the EA/PS/WOC systems towards the development of photoanodes.

2. Photochemical mechanism

The photochemical mechanism in a three component EA/PS/WOC system starts with absorption of light by PS and generation of an excited state *PS (eq. 2), followed by its reaction with the EA to give the oxidized form of the photosensitizer PS^+ (oxidative quenching) and the reduced form of the electron acceptor, EA^- (eq. 3). In order to avoid detrimental charge recombination between PS^+ and EA^-, suitable EA are those in which the reduced form is unstable and transforms into decomposition products (eq. 4).

$$PS + h\nu \rightarrow {}^*PS \quad (2)$$
$${}^*PS + EA \rightarrow PS^+ + EA^- \quad (3)$$
$$EA^- \rightarrow \text{decomposition products} \quad (4)$$

At this stage the WOC may undergo consecutive electron transfer processes to the photogenerated oxidized species of the sensitizer PS^+ (eqs. 5-8). After four oxidizing equivalents are transferred to the WOC, water oxidation to dioxygen may occur (eq. 9) and the WOC is restored back to its initial state. For the

sake of simplicity, in eqs. 5-9 proton transfer reactions among the different oxidized form of the WOC are not considered. It should be noted, however, that the possibility to undergo proton-coupled electron transfer (PCET)[38],[39],[40] events is regarded as a key feature of a WOC to access redox potential levelling among subsequent oxidized states and to drive catalysis at low overpotential.[41],[42] This last feature requires a proper design and engineering of the WOC;[10-14] low operating overpotential of the WOC is of particular relevance in the case of photoactivated cycles discussed herein, where the feasibility of activation of the WOC through the stepwise oxidation processes (eqs. 5-8) depends on the potentials of the WOC^{n+1}/WOC^{n+} couples, with respect to the potential of the PS^+/PS one.

$$PS^+ + WOC \rightarrow PS + WOC^+ \quad (5)$$
$$PS^+ + WOC^+ \rightarrow PS + WOC^{2+} \quad (6)$$
$$PS^+ + WOC^{2+} \rightarrow PS + WOC^{3+} \quad (7)$$
$$PS^+ + WOC^{3+} \rightarrow PS + WOC^{4+} \quad (8)$$
$$WOC^{4+} + 2\ H_2O \rightarrow WOC + O_2 + 4\ H^+ \quad (9)$$

The quantum yield (Φ_{O_2}) of photochemical oxygen evolution can be theoretically predicted according to eq 10.[43]

$$\Phi_{O_2} = 0.25\ (\Phi_{Ox_1} + \Phi_{Ox_2} + \Phi_{Ox_3} + \Phi_{Ox_4}) \times \eta_{WOC} \quad (10)$$
$$\Phi_{Ox_n} = \eta_{abs} \times \eta_{PS^+} \times \eta_{ET_n} \quad (11)$$
$$\eta_{PS^+} = \eta_Q \times \eta_{CS} \quad (12)$$

Φ_{Ox_n} (with n = 1-4) is described by eq 11 and represents the efficiency in the photogeneration of the WOC^{n+} catalytic intermediate (eqs. 5-8) and η_{WOC} is the oxygen evolution yield (eq. 9). η_{abs} is the efficiency of light absorption by the PS (eq. 2). η_{PS^+} represents the quantum yield of oxidant generation by photoinduced oxidative quenching of the sensitizer (eq. 3) and is given by the product of the quenching efficiency (η_Q) and the cage-escape yield (η_{CS}), according to eq 12. η_{ET_n} is the efficiency of the electron transfer from the WOC intermediates to the oxidized photosensitizer (eqs. 5-8). Being such an electron transfer a bimolecular reaction, its efficiency strictly depends on the concentration of every intermediates. Accordingly, by assuming that under steady-state irradiation conditions the concentration of the WOC resting state is dominating, the quantum yield of photochemical oxygen evolution can be approximated according to eq. 13, where η_{ET} now represents the efficiency of the electron transfer process from the resting state of the WOC to the oxidized sensitizer.

$$\Phi_{O_2} \approx 0.25\ (\eta_{abs} \times \eta_{PS^+} \times \eta_{ET} \times \eta_{WOC}) \quad (13)$$

From eq. 13 it appears immediately clear that a combination of several parameters related to both light-induced or dark (thermal) processes is at the basis of the efficiency of the overall photochemical water oxidation mechanism. Therefore, a thorough understanding and control of such reaction parameters is a key point towards efficient light-driven photocatalysis.

Before describing the PSs that have been considered in the literature for photochemical water oxidation purposes, we highlight some key features needed to achieve efficient photogeneration of PS^+ according to the reaction sequence in eqs. 2-4. (i) The PS should absorb light efficiently and possibly spanning the whole visible region (eq. 2). (ii) The excited state *PS should have a lifetime long enough to react with the EA (eq. 3), thus limiting competitive ground state decay (desirable lifetimes should span the ns-μs timescale, although this is not a stringent requirement when the PS is integrated in a sensitized photoelectrode, where electron injection may occur faster, i.e. within ps-ns).[44] To this respect, PSs displaying high triplet yields are typically the best candidates, particularly when a bimolecular reaction is considered. (iii) The potential difference $E(EA/EA^-) - E(PS^+/*PS)$ (where the potential $E(PS^+/*PS)$ is given by eq. 14)[45] has to be positive enough to provide sufficient thermodynamic driving force for eq. 3 to occur.

$$E(PS^+/*PS) = E(PS^+/PS) - E^{00} \quad (14)$$

iv) The EA should decompose efficiently upon electron transfer (eq. 4) in order to limit competitive recombination processes with the oxidized sensitizer (PS^+). Accordingly, persulfate anion $S_2O_8^{2-}$ (E = +0.6 V vs NHE for the one-electron oxidation process)[[46]] and chloropentaamminecobalt(III) dichloride $Co(NH_3)_5Cl_3$ (E = +0.52 V vs NHE)[46] are EAs typically employed, due to the fast degradation route of their one-electron reduced products (eq. 4). In particular, $S_2O_8^{2-}$ undergoes O-O bond rupture with formation of SO_4^{2-} and $SO_4^{\bullet-}$ (eq. 15) with the latter being a strong oxidant (E between 2.4-3.4 V vs. NHE)[47,48] and able to oxidize a second equivalent of PS (eq. 16). $Co(NH_3)_5Cl^{2+}$ on the other hand undergoes ligand dissociation upon Co(III) to Co(II) reduction (eq. 17).[46]

$$*PS + S_2O_8^{2-} \rightarrow PS^+ + SO_4^{2-} + SO_4^{\bullet-} \quad (15)$$
$$PS + SO_4^{\bullet-} \rightarrow PS^+ + SO_4^{2-} \quad (16)$$
$$*PS + Co(NH_3)_5Cl^{2+} \rightarrow PS^+ + Co^{2+} + 5\ NH_3 + Cl^- \quad (17)$$

It is important to point out that, according to the reactions in eqs. 15-17, the efficiency of oxidant generation (η_{PS^+}, eq. 12) may reach a maximum value of 2 and 1 for the persulfate and $Co(NH_3)_5Cl^{2+}$ EA, respectively. Therefore, the quantum yield of photochemical oxygen evolution (Φ_{O_2}) using the three-component EA/PS/WOC combination may attain maximum values up to 0.5 and 0.25 for the $S_2O_8^{2-}$ and $Co(NH_3)_5Cl^{2+}$ systems, respectively. In order to compare the performances in water oxidation photocatalysis within the two different photochemical systems it should thus be recommended to refer to the "quantum efficiency" (QE) defined in eq. 18 as the ratio between the experimental quantum yield and the theoretical maximum value (i.e., 0.5 and 0.25 for the $S_2O_8^{2-}$ and $Co(NH_3)_5Cl^{2+}$ systems, respectively).[34]

$$QE = \Phi_{O_2,\ exp} / \Phi_{O_2,\ theor} \quad (18)$$

Besides the key conditions outlined above concerning the efficient photogeneration of PS^+, the PS must satisfy additional requirements. As a matter of fact, the PS^+ form of the photosensitizer should be oxidizing enough to feed the WOC with oxidizing equivalents (eqs. 5-8, see paragraph 3). Therefore,

an important parameter to be considered is the ground-state oxidation potential E(PS^+/PS) which should be more positive than the potentials E(WOC^{+n}/WOC^{+n+1}) for consecutive one-electron oxidation of the WOC. This would indeed provide substantial exergonicity for the reactions in eqs. 5-8. Also, PS^+ should display enough stability in aqueous solution to limit competitive degradation pathways, generally associated to self-oxidation (disproportionation) and/or water nucleophilic attack.[49],[50],[46]

Key selected examples of PS employed in photochemical water oxidation with EA are represented in Figure 1, while their relevant photophysical and electrochemical properties are summarized in Table 1.

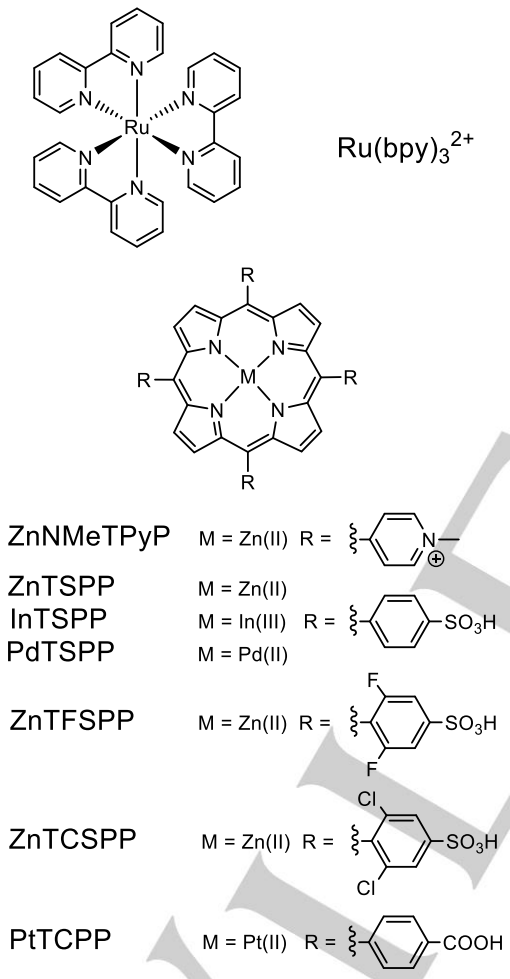

Figure 1. Molecular structure of the PSs employed in photochemical water oxidation studies.

The prototype PS used in light-driven water oxidation studies is the well-known $Ru(bpy)_3^{2+}$ (where bpy = 2,2'-bipyridine) that combines all the key requirements, namely high absorption in the visible range, unitary triplet yield, and long excited state lifetime to promote bimolecular electron transfer processes, suitable excited state reduction potential and ground-state oxidation potential to favor oxidative quenching by the EA and activation of the WOC, respectively.[51] Importantly, photoinduced oxidative quenching of $*Ru(bpy)_3^{2+}$ by both $S_2O_8^{2-}$ and $Co(NH_3)_5Cl^{2+}$ sacrificial reagents turns out to be also kinetically favored and efficient. Although the experimental conditions play an important role in the quenching processes,[52],[53] quantitative yields for PS^+ photogeneration (η_{PS^+}) are potentially achievable using such a metal complex.[54],[55] Even if the stability of the Ru(III) species is limited particularly at neutral to basic pH,[49,50] this peculiar photophysical and electrochemical properties made $Ru(bpy)_3^{2+}$ the PS of choice for most of the photocatalytic water oxidation studies accomplished by far. Also, simple functionalization of the bipyridine ligands may easily allow for a convenient adjustment of the redox potentials while keeping comparable photophysical properties. For instance, the ruthenium complex $Ru(bpy)(bpyCOOEt)_2^{2+}$ (where bpyCOOEt = 4,4'-ethyl ester dicarboxylate-2,2'-bypyridine) was used as a photosensitizer in some photochemical water oxidation studies in order to exploit a more powerful oxidizing Ru(III) species than attainable with $Ru(bpy)_3^{3+}$ (E = +1.62 V vs NHE).[56,57] This, however, occurs at the expenses of a loss in terms of PS^+ photogeneration yield (η_{PS^+}).

Other types of dyes employed for photocatalytic water oxidation belong to the class of water-soluble metalloporphyrins. These chromophores generally possess some advantages over $Ru(bpy)_3^{2+}$ combining good absorption properties throughout the visible spectrum until 600 nm with high extinction coefficients. Also, triplet yields are almost close to unity and related excited state lifetime substantially long to favor oxidative quenching by the EA. However, metalloporphyrins present several drawbacks that prevent the widespread exploitation of such chromophores with respect to the ruthenium-based counterpart. The potential of the PS^+/PS couple is in general less positive than that of $Ru(bpy)_3^{3+/2+}$ thus hampering, in some cases, activation of WOCs operating at high potentials; in these cases, working under alkaline conditions may allow to reach the suitable driving force to activate the catalytic process, as in the case of ZnTSPP ($E_{1/2}$ for $ZnTSPP^+$/ZnTSPP = +0.87 V vs NHE, used as the PS with colloidal iridium oxides as the WOC, at pH 11).[58] A similar Zn-porphyrin was also used with iridium oxide colloids WOC, when templated in genetically engineered virus scaffolds.[59] Besides this low oxidative power, as a consequence of the low energy of the triplet excited state (ca 1.6 eV for the Zn(II), In(III) regular porphyrins, ca 1.8 eV in the case of the Pt(II), Pd(II) hypso-type analogs),[60],[61] the reduction potential of the triplet excited state is more positive than that of $*Ru(bpy)_3^{2+}$, resulting in typically reduced reactivity towards EA and consequent low PS^+ photogeneration yields.[58],[62] As a representative case, the low reducing ability of the triplet excited state of ZnNMeTPyP (E = −0.45 V vs NHE) with respect to $^{3*}Ru(bpy)_3^{2+}$ (E = −0.84 V vs NHE) leads to a decrease by two orders of magnitude of the bimolecular rate constant for persulfate quenching of the former with respect to the latter.[62] Finally, porphyrin photosensitizers and their radical cations are favorably prone to degradation routes. In particular, using persulfate as the sacrificial agent, dark (thermal) degradation of the macrocycle is observed in

some cases, thus additionally limiting their applicability in photochemical water oxidation studies.[58],[62] Interestingly, a particular case to this respect is represented by the platinum porphyrin (PtTCPP) featuring peripheral benzoic acid groups (and thus deprotonated in neutral aqueous media) for which efficient water oxidation ability in an EA/PS/WOC system was recently reported.[63] The PS^+ species of this chromophore displays indeed a substantially high oxidation power, even better than $Ru(bpy)_3^{3+}$ (E = +1.42 V vs NHE, see Table 1), while keeping enhanced stability *via* charge compensation by the benzoate moieties.[63] This is indeed the only case where photochemical water oxidation using a metalloporphyrin as PS was found to compare well with that driven by $Ru(bpy)_3^{2+}$.

Table 1. Photophysical and electrochemical properties of photosensitizers considered for water oxidation within sacrificial cycles with electron acceptors.

PS	Abs λ, nm (ε, $M^{-1}cm^{-1}$)	E^{00}, eV[a]	Triplet yield	Lifetime, μs[b]	E (PS^+/PS), V vs NHE
$Ru(bpy)_3^{2+}$ [c]	450 (1.4×10^4)	2.12	1	0.58	+1.26
ZnTMePyP[d]	436 (1.8×10^5), 562 (1.6×10^4)	1.63	0.9	1300 (650)[g]	+1.18
PtTCPP[e]	395 (2.1×10^5), 511 (1.7×10^4), 542 (2.7×10^3)	1.82	1	9	+1.42
PdTSPP[d]	412 (1.3×10^5), 520 (1.0×10^4)	1.86	1	350	+1.09
ZnTSPP[d]	421 (6.8×10^5), 555 (2.1×10^4), 594 (9.6×10^3)	1.61	0.84	1400 (210)[f]	+0.87
ZnTFSPP[f]	419 (5.8×10^5), 552 (1.8×10^4), 589 (3.4×10^3)	1.57	0.88	60	+1.00
ZnTCSPP[f]	423 (6.9×10^5), 556 (2.4×10^4), 590 (2.1×10^3)	1.58	0.92	165	+1.02
InTSPP[f]	418 (6.4×10^5), 516 (3.6×10^3), 557 (2.3×10^4), 594 (1.1×10^4)	1.64	0.95	90	+1.16

[a] triplet excited state energy; [b] measured in deoxygenated aqueous solution; [c] taken from ref. [64]; [d] taken from ref. [65]; [e] taken from ref. [63]; [f] taken from ref. [58]; [g] taken from ref. [66].

3. Electron transfer rate from WOC to PS^+

As described in paragraph 2, the quantum yield of photochemical water oxidation (Φ_{O_2}) is determined, in first approximation, by the product of different contributions (eq. 13), namely the light-absorption efficiency (η_{abs}), the yield of oxidized photosensitizer (η_{PS^+}), the electron transfer efficiency (η_{ET}), and the oxygen evolution yield (η_{WOC}). In general, η_{abs} can be kept constant by working under comparable light intensities and close to unity by raising the PS concentration. η_{PS^+} strictly depends on the experimental conditions adopted. For instance, within the $Ru(bpy)_3^{2+}/S_2O_8^{2-}$ sacrificial system, its value depends on the persulfate concentration, on the ionic strength of the solution, and on the presence (and content) of organic co-solvents.[52],[53] Under comparable experimental conditions, however, η_{PS^+} can be confidently regarded as a constant regardless of the WOC employed. Also, η_{WOC} can be considered close to unity for active WOCs, this parameter being closely related to the Faradaic efficiency under electrochemically-driven catalysis.[57] Hence, under these assumptions and according to eq. 13, the efficiency of the electron transfer from the WOC to the oxidized sensitizer (η_{ET}) plays a key role in the overall photocatalytic efficiency. Its value can be described according to eq. 19, where k_{ET} is the bimolecular rate constant for the electron transfer reaction (hole scavenging) and k_0 is related to deactivation routes of the oxidized sensitizer.

$$\eta_{ET} = k_{ET}[WOC] / (k_{ET}[WOC] + k_0) \quad (19)$$

It appears immediately clear that the faster the electron transfer from the WOC to the oxidized chromophore, the higher the η_{ET}, with positive impact on the efficiency and stability of the photocatalytic system. Moreover, fast electron transfer rates from WOC to PS^+ are crucial in regenerative systems (namely dye-sensitized photoanodes based on wide band-gap n-type semiconductors) where the WOC must be able to transfer the electron to the oxidized photosensitizer in competition with charge recombination (see paragraph 6). Therefore, according to these considerations, the determination of the bimolecular rate constant of the electron transfer process from the WOC to the oxidized dye turns out to be an important task towards the identification and optimization of suitable catalysts capable of efficient water oxidation.

Nanosecond laser flash photolysis can be conveniently exploited for the determination of the bimolecular rate constant for the primary electron transfer from the WOC to PS^+. In these experiments a given concentration of oxidized photosensitizer is generated within few ns with a laser pulse that triggers the bimolecular oxidative quenching of the excited chromophore *PS by the EA (eq. 3). The reduction of the oxidized sensitizer by the WOC (eq. 5) can be then followed over a relatively wide time-window (ca 100 ms). In the $Ru(bpy)_3^{2+}/S_2O_8^{2-}$ system typically employed, the formation of the oxidized Ru(III) sensitizer is detected as a bleach (negative ΔOD signal) of the metal-to-ligand charge-transfer (MLCT) transition of the chromophore centered at 450 nm. Using persulfate as sacrificial acceptor, this formation is in fact biphasic with a first, prompt contribution arising from direct photochemical quenching (eq 15) and a second, delayed contribution (typically few μs) deriving from the thermal reaction of the photogenerated sulfate radical with other (ground-state) $Ru(bpy)_3^{2+}$ molecules in solution (eq 16).[53] In the absence of any catalyst, the photogenerated oxidized Ru(III) species does not evolve to an appreciable extent within the time-window of the flash photolysis experiment. This can be clearly observed from the apparent persistence of the bleaching at 450 nm over the whole time-scale examined (see as an example the

black trace in Figure 2A). In the presence of the WOC, the increase of the ΔOD signal at 450 nm observed overtime (i.e., bleach recovery of the MLCT absorption) is indicative of the occurrence of the Ru(III)→Ru(II) reduction by the WOC, that concomitantly gets oxidized (eq. 5). This is the situation typically encountered in the laser flash photolysis experiments since the difference in molar extinction coefficient (Δε) at 450 nm between the WOC and WOC^+ is in general lower than that of $Ru(bpy)_3^{3+}$ (Δε = 13,000 $M^{-1}cm^{-1}$ at 450).[67] In most cases, this difference is even negligible and the negative ΔOD signal is thus recovered until a ΔOD = 0 is reached (colored traces in Figure 2A). In some cases, however, positive or negative permanent ΔOD values may be observed upon Ru(III) bleach recovery and are indicative of the formation of the WOC^+ intermediate upon hole scavenging (see below, paragraph 5). Importantly, the kinetics of bleach recovery are dependent on the concentration of the WOC, with faster rates paralleling higher catalyst amounts (Figure 2A). The bimolecular rate constant for the electron transfer (k_{ET}) can be then estimated under pseudo-first order kinetic conditions (i.e., [WOC] >> [Ru(III)]), where the rates of bleach recovery (k_{obs}, estimated from exponential fitting of the kinetic traces) are linearly dependent on the WOC concentration (Figure 2B).

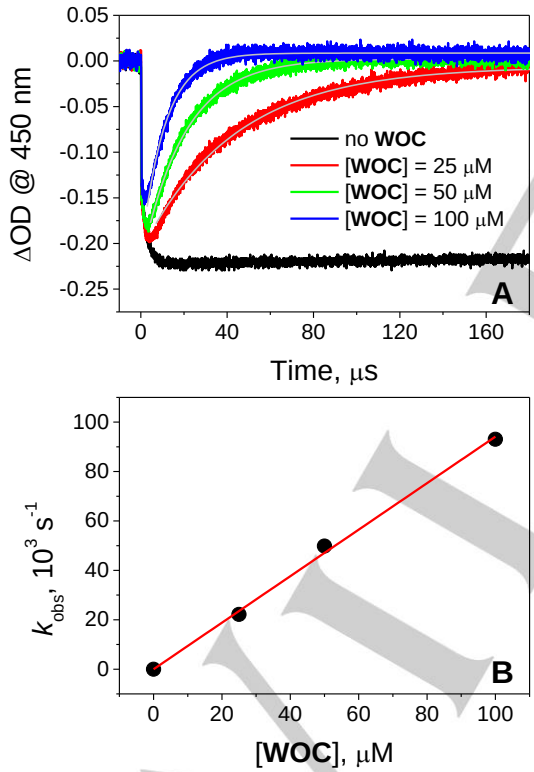

Figure 2. (A) Kinetic traces at 450 nm obtained by laser flash photolysis (excitation at 355 nm) of 20 mM phosphate buffer (pH 8) solutions containing 50 μM $Ru(bpy)_3Cl_2{\cdot}6H_2O$, 5 mM $Na_2S_2O_8$, and 0-100 μM Co_7POM as the WOC. (B) Plot of the rates of bleach recovery (obtained from single exponential fitting of the kinetic traces) vs. WOC concentration, the slope of the linear correlation gives the bimolecular rate constant k_{ET}. Adapted from reference [68] with permission from Elsevier.

The bimolecular rate constant for a series of WOCs (selected examples are represented in Figure 3) involving photogenerated $Ru(bpy)_3^{3+}$ as the electron transfer acceptor are collected in Table 2.

Table 2. Bimolecular rate constants of electron transfer from the WOC to photogenerated $Ru(bpy)_3^{3+}$. Experimental conditions and references are also indicated.

WOC	k_{ET} [$M^{-1}s^{-1}$]	Conditions [a]	Reference
IrO_x	1.3×10^6	SBB, pH 5.7	[49]
$Ale@Co_3O_4$	~6×10^4	PB, pH 8	[68]
Co_3O_4	5.3×10^5	PB, pH 8	[68]
Ru_4POM	3.6 (±0.1) × 10^9	PB, pH 7	[69,70]
Co_7POM	9.4 (±0.3) × 10^8	PB, pH 8	[68]
Co_9POM	2.1 (±0.3) × 10^9	PB, pH 8	[71]
$Co_{15}POM$	5.0 (±0.4) × 10^9	PB, pH 8	[71]
$Co_{16}POM$	4.5 (±0.4) × 10^9	PB, pH 8	[71]
Mn_4POM	4.6 (±0.6) × 10^6	SBB, pH 5.2	[72]
$V_6O_7(OCH_3)_{12}^-$	2.5 (±0.2) × 10^8	ACN/PB, pH 7 [b]	[73]
Co_4O_4 -H	1.2 (±0.4) × 10^7	PB, pH 7	[74]
Co_4O_4 -H	1.6 (±0.4) × 10^7	BB, pH 8	[74]
Co_4O_4 -H	2.1 (±0.1) × 10^8	ACN/BB, pH8 [b]	[75]
Co_4O_4 -Me	2.7 (±0.1) × 10^8	ACN/BB, pH8 [b]	[75]
Co_4O_4 -OMe	3.7 (±0.3) × 10^8	ACN/BB, pH8 [b]	[75]
Co_4O_4 -*t*Bu	2.3 (±0.1) × 10^8	ACN/BB, pH8 [b]	[75]
Co_4O_4 -Br	9.6 (±0.7) × 10^7	ACN/BB, pH8 [b]	[75]
Co_4O_4 -COOMe	6.0 (±0.3) × 10^7	ACN/BB, pH8 [b]	[75]
Co_4O_4 -CN	2.3 (±0.2) × 10^7	ACN/BB, pH8 [b]	[75]
Co_4O_4 ‘	2.4 (±0.1) × 10^8	ACN/PB, pH8 [b]	[76]
CoSIp	1.1 × 10^8	PB, pH 8	[77]
Ru1	2.4 × 10^8	PB, pH 7	[78]
Ru2 [c]	~1 × 10^9	ACN/BB, pH 8 [d]	[79]
Ru3 [e]	1.4 × 10^7	PB, pH 7	[57]

[a] PB = phosphate buffer, BB = borate buffer, SBB = hexafluorosilicate/ bicarbonate buffer, ACN = acetonitrile, for the exact concentration of buffers the reader is referred to the original reference; [b] 1/1 ratio; [c] $Ru(bpy)_2(bpyp)^{2+}$ (where bpyp = 2,2’:4’,4’’-terpyridine) was used as a photosensitizer; [d] 1/9 ratio; [e] $Ru(bpy)(bpyCOOEt)_2^{2+}$ (where bpyCOOEt = 4,4’-ethyl ester dicarboxylate-2,2’-bypyridine) was used as a photosensitizer, the electron transfer rate is related to a Ru(IV)=O intermediate of the WOC.

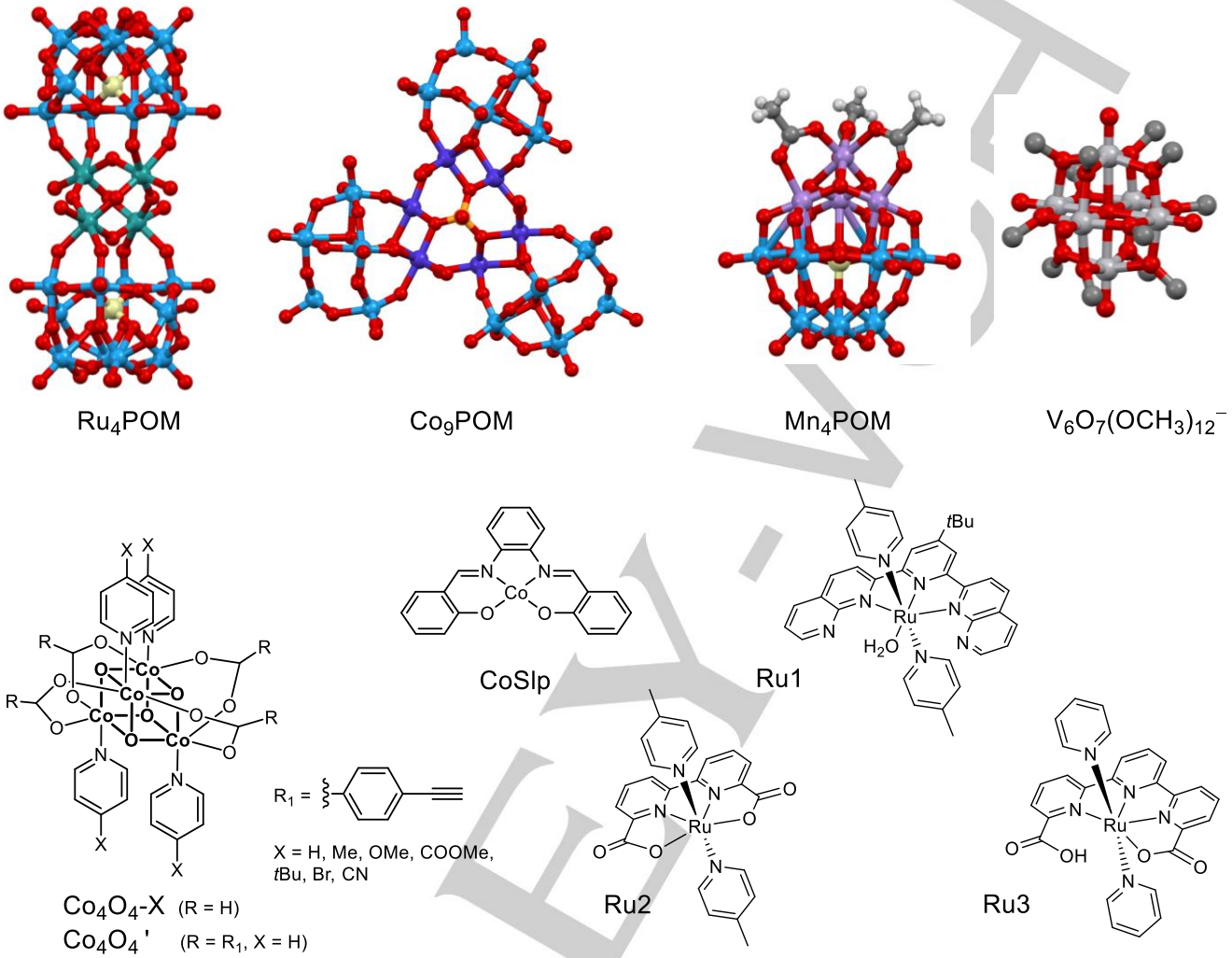

Figure 3. Representation of selected WOCs discussed in this paragraph. Colour code for the POM complexes: green, Ru; red, O; sky blue, W; light yellow, Si; dark blue, Co; orange, P; purple, Mn; dark grey, C; light grey, V; white, H (additional hydrogen atoms have been omitted for clarity reasons).

While laser flash photolysis experiments conducted under pseudo-first order conditions can give information on the electron transfer rate from the initial state of the WOC to the photogenerated oxidant, further details on the kinetics of the subsequent electron transfer processes (i.e., to those intermediates involved in the overall water oxidation mechanism) can be obtained by working under slightly different experimental conditions. For instance, in the $Ru(bpy)_3^{2+}/S_2O_8^{2-}$ system, by following the bleach recovery at 450 nm in the presence of a sub-stoichiometric (with respect to the photogenerated oxidant) amount of catalyst, it is in principle possible to determine the number of electron transfer processes performed by the WOC during a sufficiently long time-window (up to ca 100 ms).[68,70–72] Although pure kinetic constants cannot be extracted from this investigation, this experiment sets a lower limiting value for the kinetics of the subsequent (if any) electron transfer processes from the WOC to the photogenerated oxidant.

One of the first WOC examined in a mechanistic perspective was the colloidal iridium oxide (IrO_x) reported by Mallouk and coworkers.[49] A bimolecular rate constant $k_{ET} = 1.3\times10^6$ $M^{-1}s^{-1}$ was measured for the oxidation of Ir(IV) sites by the photogenerated Ru(III) oxidant. The small value of k_{ET} estimated for such an electron transfer (bimolecular k_{ET} is more than three orders of magnitude lower than diffusion controlled reactions) was such that this oxidation process was recognized as the rate determining step in photoinduced water oxidation catalysis by IrO_x nanoparticles.[49] As expected, this apparent inertness has profound implications on the stability of the photocatalytic system during photoirradiation. Enhanced dye degradation was indeed observed upon photolysis in phosphate buffer solution,

while an improved stability was only attained using a non-coordinating buffer based on the $Na_2SiF_6/NaHCO_3$ combination.[80] Interestingly, this slow response towards electron transfer to Ru(III) was preserved even upon grafting of the sensitizer onto the IrO_x surface,[81] and was indeed identified as a major source of inefficiency in the operation of a dye-sensitized photoanode coupling mesoporous TiO_2 with such PS/WOC system.[82] Slow bimolecular electron transfer rates to photogenerated $Ru(bpy)_3^{3+}$ were also measured for other metal oxides such as Co_3O_4 nanoparticles both *"as prepared"* (i.e., with no stabilizing ligands) and when capped with organic alendronate pendants (Ale@Co_3O_4).[68] Similarly slow kinetics were observed for core-shell nanoparticles featuring a Co_3O_4 core embedded with a thin silica layer.[83]

If slow electron transfer appears as an intrinsic characteristic of metal oxide phases, fast kinetics towards photogenerated Ru(III) were, on the other hand, typically encountered using the molecular "metal-oxide" analogs, namely polyoxometalate (POM) metal-oxo clusters. Bimolecular rate constants close to the diffusion-controlled regime were experimentally measured for the tetraruthenium POM $\{Ru_4(\mu\text{-}O)_4(\mu\text{-}OH)_2(H_2O)_4[\gamma\text{-}SiW_{10}O_{36}]^{10-}$, Ru_4POM, (k_{ET} = 3.6×10^9 $M^{-1}s^{-1}$)[69,70] and polynuclear cobalt POMs $[\{(B\text{-}\alpha\text{-}PW_9O_{34})Co_3(OH)(H_2O)_2(O_3PC(O)(C_3H_6NH_3)PO_3)\}_2Co]^{14-}$ (Co_7POM), $[Co_9(H_2O)_6(OH)_3(PW_9O_{34})_3]^{16-}$ (Co_9POM), $[Co_6(H_2O)_{30}\{Co_9Cl_2(OH)_3(H_2O)_9(SiW_8O_{31})_3\}]^{5-}$ ($Co_{15}POM$), and $[\{Co_4(OH)_3PO_4\}_4(PW_9O_{34})_4]^{28-}$ ($Co_{16}POM$), with k_{ET} = 0.9 – 5.0 $\times10^9$ $M^{-1}s^{-1}$, see Table 2.[68],[71] This enhanced electron transfer ability turns out to be a peculiar figure of merit of this class of molecular WOCs enabling sustained oxygen evolution, e.g., with quantum yields up to 4.5% and 5.5% for Ru_4POM and $Co_{15}POM$, respectively (corresponding to 9% and 11% overall quantum efficiency, respectively).[71,84] Furthermore, experiments conducted under sub-stoichiometric WOC concentrations point towards the occurrence of a very fast multi-hole accumulation upon sequential electron transfer processes at the basis of the efficient water oxidation catalysis.[70,71] While these features well apply to the ruthenium and cobalt POMs, a substantially low second-order rate constant was measured for the electron transfer to $Ru(bpy)_3^{3+}$ from the mixed-valent tetra-manganese complex $[Mn^{III}_3Mn^{IV}O_3(CH_3COO)_3(A\text{-}\alpha\text{-}SiW_9O_{34})]^{6-}$ Mn_4POM (k_{ET} = 4.6×10^6 $M^{-1}s^{-1}$),[72] an artificial WOC designed to mimic the active site of the natural OEC.[85–87] Possible reasons accounting for this evidence were ascribed to the large reorganization energy accompanying the Mn(III)→Mn(IV) oxidation which, in the present case, very likely involves a partial displacement of the pendent acetate ligands. Consistently, the water oxidation activity within the photochemical $Ru(bpy)_3^{2+}/S_2O_8^{2-}$ cycle was indeed relatively modest, with a quantum efficiency for oxygen production of 1.7%.[72]

Moderate electron transfer rates were measured in aqueous solutions for the cubane complex Co_4O_4-H (k_{ET} = 1.2-1.6 $\times10^7$ $M^{-1}s^{-1}$),[74,88] used as molecular model of the CoPi electrocatalyst designed by Kanan and Nocera.[89,90] An important enhancement of these rates (by ca one order of magnitude) was then made possible by simply changing the solvent to an acetonitrile/water mixture (see Table 2),[75],[58] mainly ascribable to the increased driving force for the oxidation process in the new conditions. More interestingly, alteration of the electron transfer rates within the same Co_4O_4 system was achieved by suitable substitutions in the *para* position of the pyridine ligands (Co_4O_4-X in Figure 3).[75] A linear free-energy relationship (LFER) was attained by plotting the log (k_X/k_H) vs. the Hammett parameter of the substituents providing a negative slope indicating that electron transfer to Ru(III) is favored by the presence of electron donating groups on the pyridine (Figure 4).

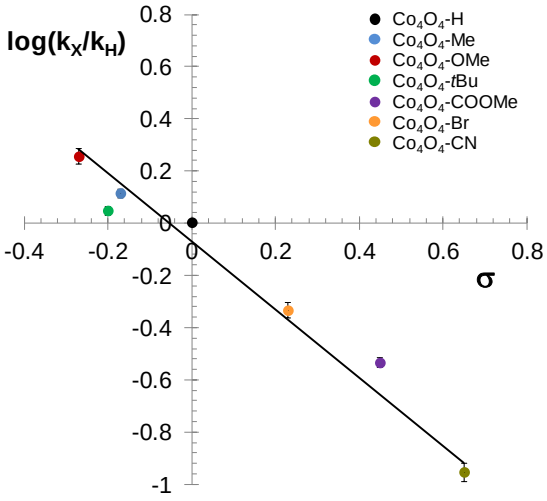

Figure 4. Hammett plot of the electron transfer rate from Co_4O_4-X to photogenerated Ru(III) oxidant. Adapted with permission from reference [75]. Copyright 2012 American Chemical Society.

Comparable bimolecular electron transfer rates approaching the diffusion limit were measured for a series of other molecular WOCs. These include single-site molecular catalysts such as the ruthenium(II) complexes Ru1 and Ru2 (k_{ET} = 2.4×10^8 $M^{-1}s^{-1}$ and ~1×10^9 $M^{-1}s^{-1}$, respectively)[78],[79] and the cobalt(II) complex CoSlp (k_{ET} = 1.1×10^8 $M^{-1}s^{-1}$).[77] Interestingly, in the latter system, flash photolysis experiments performed under sub-stoichiometric conditions ([CoSlp] << [Ru(III)]) clearly reveal that both Co(II)→Co(III) and Co(III)→Co(IV) oxidations are relatively fast (within the ms time-scale) and the kinetic bottleneck in water oxidation catalysis by CoSlp is most likely the O-O bond formation.[77] A similar rate constant (k_{ET} = 2.5×10^8 $M^{-1}s^{-1}$) was also recorded for the electron transfer to Ru(III) from the first WOC ever reported containing vanadium as the active metal center ($V_6O_7(OCH_3)_{12}^-$, see Figure 3).[73]

A lower rate (k_{ET} = 1.4×10^7 $M^{-1}s^{-1}$) was measured for the oxidation of the Ru(IV)=O resting state of a highly active single-site ruthenium complex Ru3.[57] Due to the appreciably high value for such an electron transfer process the authors concluded that the overall quantum yield of oxygen evolution by Ru3 is actually limited by the photogeneration of the Ru(III) oxidant.[57] In this case, however, a different sensitizer was used, namely $Ru(bpy)(bpyCOOEt)_2^{2+}$ (where bpyCOOEt = 4,4'-ethyl

ester dicarboxylate-2,2'-bypyridine), which makes the comparison with other reported systems not so straightforward.
The bimolecular rate constants for the WOCs collected in Table 2 were always determined under experimental conditions (i.e, buffer type, concentration, and pH) in which photocatalysis by the WOC is efficient. Although the absolute value of the rate constant is important, for the reasons outlined above, little is known about the actual mechanism involving the electron transfer from the WOC to the photogenerated oxidant. Interestingly, a detailed investigation of the electron transfer process from Co_3O_4 nanoparticles to photogenerated Ru(III) was recently accomplished by suitably changing the experimental conditions. It was demonstrated that the primary electron transfer process from Co_3O_4 to $Ru(bpy)_3^{3+}$ in borate buffer solution displays a strong dependence on the buffer concentration and pH.[92] This is attributed to the involvement of a proton-coupled oxidation of Co(III)-OH surface sites to Co(IV)=O assisted by a general base catalysis by the $B(OH)_4^-$ base (Figure 5) with a kinetic law expressed by eqs. 20 and 21, yielding k_B = ~7×10^2 M^{-1}s^{-1}, k_{OH} = 5.5×10^5 M^{-1}s^{-1}, and k_{H_2O} = 1.7 s^{-1}.

$$k_{obs} = k' + k_B \times [\text{Base}] \quad (20)$$
$$k' = k_{H_2O} + k_{OH} \times [OH^-] \quad (21)$$

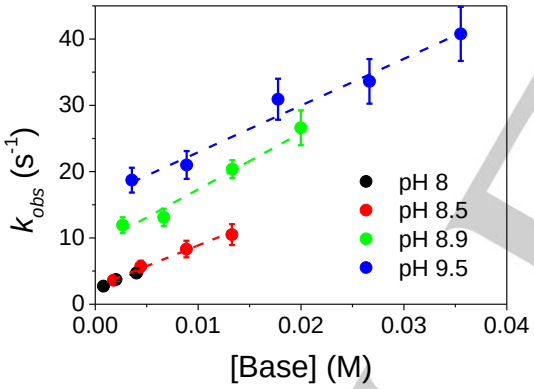

Figure 5. Plot of the electron transfer rate (k_{obs}) from Co_3O_4 nanoparticles to $Ru(bpy)_3^{3+}$ vs. base concentration measured at different pH and borate buffer concentrations (base stands for $B(OH)_4^-$ and the concentrations are given by [Base] = f_B × [buffer], where f_B is the fraction of the basic form of the buffer in solution, estimated considering a pK_a = 8.6 for the $H_3BO_3/B(OH)_4^-$ couple, and [buffer] is the total buffer concentration). Adapted from reference [92] with permission from the Royal Society of Chemistry.

Additionally, inhibition of the proton-coupled electron-transfer process was observed at high borate buffer concentrations, likely due to coordination of H_3BO_3 to cobalt surface sites, supporting previous observations on electrocatalysis by cobalt oxides.[93] Consistently, a decrease of photoinduced oxygen evolution was observed at high buffer concentrations. This work thus exemplifies how, in view of photocatalysis optimization, the determination of the rate of the electron transfer from the WOC to the photogenerated oxidant is an important task as it is (at almost the same level of importance) the understanding of the mechanism at the basis of such charge transfer reaction.
It is worth mentioning that strategies have been pursued in order to overcome the slow electron transfer from Co_3O_4 nanoparticles. In particular, Frei and coworkers designed the covalent anchoring of molecular wires to the oxide surface, based on redox-active *p*-oligo(phenylenevinylene) with three aryl units (PV3).[94] In the presence of photogenerated Ru(III) polypyridine species in solution, electron transfer from the Co_3O_4 nanoparticle to Ru(III) occurs within 1 μs and is proposed to be mediated by the surface anchored $PV3^+$ radical cation of the linker. Further engineering of the system involved the use of a 2-nm thin silica layer covering the Co_3O_4 nanoparticles, to act as gas impermeable physical barrier, while maintaining electron conductivity through the molecular wires.[83] In this asset, photoinduced electron transfer from the Co_3O_4 surface to the excited state of an electrostatically adsorbed porphyrin dye occurs in 255±23 ps (Figure 6).[95] Sala and coworkers proposed the design of 3-nm sized Co_3O_4 nanoparticles decorated with Ru(II) polypyridine based photoactive pendants.[96] This hybrid system is active in photochemical water oxidation in the presence of $S_2O_8^{2-}$, while the non-linked components are not. Fast electron transfer from Co_3O_4 to anchored photogenerated Ru(III) was thus proposed, although the rate could not be measured through flash photolysis.

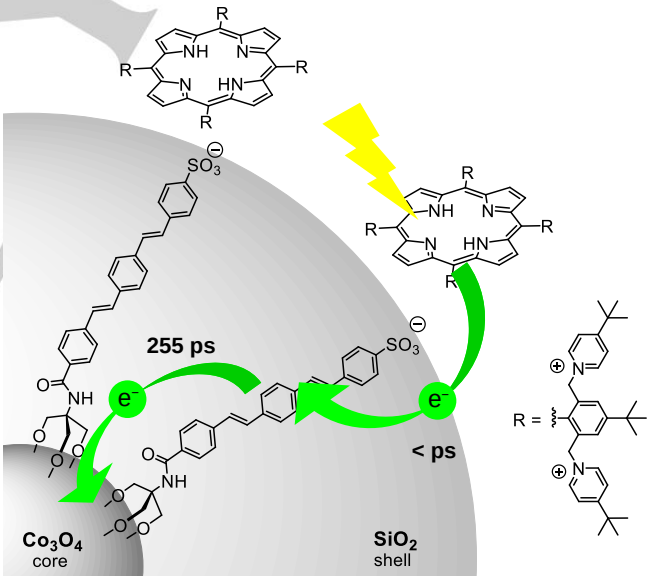

Figure 6. Structure and photoinduced electron transfer processes of Co_3O_4-SiO_2 core-shell nanoparticles embedding PV3 units and electrostatically absorbed cationic porphyrins. Adapted with permission from reference [95]. Copyright 2017 American Chemical Society.

4. Quenching and side-processes, alternative mechanisms

Besides the recognized photoactivated mechanism represented in eqs. 2-9, other processes may compete and impact on the

overall efficiency of the system. First of all, light absorption by the WOC, competing with PS, could lower the overall quantum yield. This process is however scarcely relevant due to the high extinction coefficient of the PS, and to the low WOC concentration typically employed. More important are degradation routes of the PS, often associated to self-bleaching from the oxidized form PS^+ (eq. 22), caused by its high oxidizing power.

$PS^+ \rightarrow$ degradation products (22)

These routes have been extensively investigated for the $Ru(bpy)_3^{2+}$ photosensitizer, since the oxidized form $Ru(bpy)_3^{3+}$ has a relatively high oxidation power (E = +1.26 V vs NHE for the 3+/2+ couple, see paragraph 2) and is unstable in neutral or basic aqueous solutions, partly undergoing irreversible decomposition following a first-order decaying kinetics, with overall rates depending on the solution pH and buffer nature.[49,50] The degradation process involves hydroxylation of the bpy ligands and consequent loss of photochemical activity; indeed, oxygen production usually stops due to $Ru(bpy)_3^{2+}$ decomposition.

A further side process is the quenching of *PS by the WOC, that may compete with the expected *PS quenching by the EA (eq. 3). However, considering the high EA concentrations (with respect to the WOC) typically employed in photocatalytic water oxidation experiments, oxidative quenching of *PS by EA is generally highly efficient and thus *PS quenching by the WOC is often negligible. On the other hand, quenching of *PS by the catalyst may become potentially competitive when specific interactions between the PS and the WOC are present. Quenching of the excited state of the PS is observed in chromophore-catalyst dyads obtained by combination of a $Ru(bpy)_3^{2+}$-type PS and both $Ru(tpy)(bpy)(H_2O)$ (where tpy = 2,2':6',2"-terpyridine) and $Ru(Mebimpy)(bpy)(H_2O)$ (where Mebimpy = 2,6-bis(1-methylbenzimidazol-2-yl)pyridine) WOCs, either covalently linked or supramolecularly assembled.[97],[98] In these systems, quenching of the Ru(II) PS excited state takes place through electronic energy transfer to the Ru-WOC (eq. 23) and competes with the expected photoinduced electron transfer to the acceptor.[97],[98] *PS quenching was also observed within a covalent dyad based on a $Ru(bpy)_3^{2+}$-type PS and a Co-salophen WOC.[99]

*PS + WOC $\rightarrow$ PS + *WOC (23)
(observed when PS = $Ru(bpy)_3^{2+}$-type, and WOC = $Ru(tpy)(bpy)(H_2O)$ or $Ru(Mebimpy)(bpy)(H_2O)$)

Another example of *PS quenching by the WOC is typically observed when polyoxometalate clusters are used as catalysts in combination with $Ru(bpy)_3^{2+}$ as the PS. In these systems, efficient electrostatic association between the polyanionic WOCs and the positively charged $Ru(bpy)_3^{2+}$ occurs in aqueous media at moderate ionic strength.[68,70,71] In particular, the mechanism of the quenching process was investigated in details in the case of the tetranuclear ruthenium POM (Ru_4POM) as the WOC, where efficient excited state quenching within such ionic adducts was observed in a timescale of few ps, and shown to involve reduction of the Ru_4POM with concurrent oxidation of the PS (eq. 24).[70]

*PS + WOC $\rightarrow$ PS^+ + WOC^- (24)
(observed with PS = $Ru(bpy)_3^{2+}$ and WOC = Ru_4POM)

Hence, the formation of ion pairs results in an energy wasting process which is detrimental towards photocatalytic water oxidation. Indeed, this process competes effectively with the oxidative quenching of *PS by the EA thus appreciably decreasing the PS^+ formation yield (η_{PS^+}) and eventually the overall oxygen quantum yield (Φ_{O_2}). Accordingly, the minimization of the ion-pair association between Ru_4POM and $Ru(bpy)_3^{2+}$, by increasing the ionic strength and/or lowering the WOC-to-PS ratio, turns out to be an important requirement to promote efficient light-driven water oxidation.[84]

If ground-state association between the $Ru(bpy)_3^{2+}$ PS and the Ru_4POM WOC leads to undesired, detrimental quenching pathways, a different situation is encountered when a tetranuclear ruthenium dendrimer $[Ru\{(\mu\text{-}2,3\text{-}dpp)Ru(bpy)_2\}_3]^{8+}$ (μ-2,3-dpp = 2,3-bis(2-pyridyl)pyrazine), hereafter Ru4, is used as the PS (Figure 7).[100–103] In this compound, the excited state redox potentials (for Ru4: $E_{PS^+/*PS}$ = −0.03 V vs NHE; E_{*PS/PS^-} = +1.38 V vs NHE; for $Ru(bpy)_3^{2+}$: $E_{PS^+/*PS}$ = −0.86 V vs NHE; E_{*PS/PS^-} = +0.84 V vs NHE)[104] are indeed suitably unbalanced in order to make reductive quenching thermodynamically more favored than a potentially competing oxidative one. As a matter of fact, the primary photochemical event in photoinduced water oxidation within the $S_2O_8^{2-}$/Ru4/Ru_4POM system is a reductive photoinduced electron transfer from the Ru_4POM WOC to the triplet excited state of Ru4 (eq. 25) followed by electron scavenging by the persulfate sacrificial acceptor (eq. 26).[104]

*PS + WOC $\rightarrow$ PS^- + WOC^+ (25)
PS^- + EA $\rightarrow$ PS + EA^- (26)
(observed with PS = Ru4, WOC = Ru_4POM, EA = $S_2O_8^{2-}$)

In short, in the case of Ru_4POM as the WOC, while ionic association with $Ru(bpy)_3^{2+}$ PS leads to oxidative, unproductive quenching of *PS (eq. 24), ionic association with Ru4 leads to reductive, productive quenching of *PS (eq. 25). To this respect, ground-state electrostatic association between the reactants[105] turns out to be an important requisite in order to speed up the electron transfer processes needed to drive the overall photoreaction. Also, the possibility of the photochemical system to cycle through the reduced state of the PS (rather than through the oxidized state, as in the case of $Ru(bpy)_3^{2+}$) may pose some benefits as far as stability issues are concerned.[49,50]

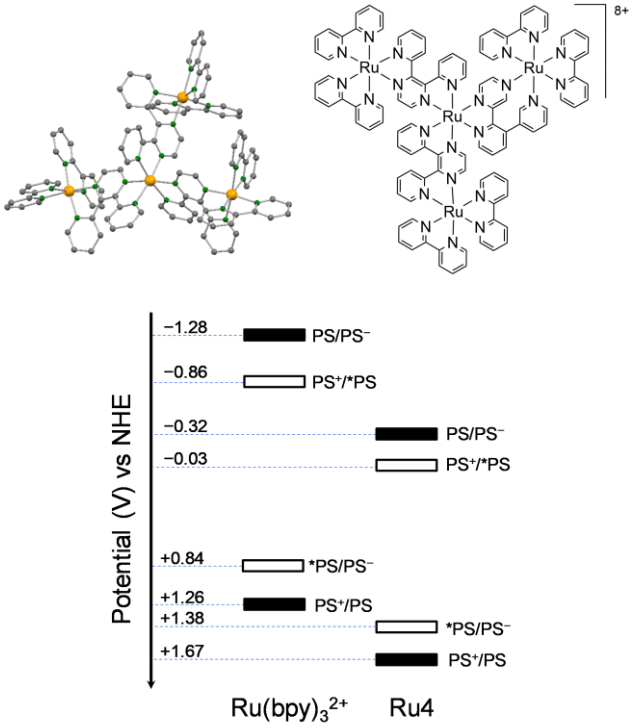

Figure 7. Top: ball-and-stick representation and molecular formula of the tetranuclear ruthenium dendrimer Ru4 $[Ru\{(\mu\text{-}2,3\text{-}dpp)Ru(bpy)_2\}_3]^{8+}$ (where μ-2,3-dpp = 2,3-bis(2-pyridyl)pyrazine and bpy = 2,2'-bipyridine). Bottom: redox potential of ground (black filled rectangles) and excited states (empty rectangles) of $Ru(bpy)_3^{2+}$ and Ru4.

5. Photogenerated WOC intermediates

The results presented in previous paragraphs 3 and 4 are based on techniques that follow spectral features of the PS. Complementary mechanistic information can be obtained by characterization of WOC intermediates, by means of transient spectroscopies combined to flash photolysis experiments. It is worth recalling that the fast generation and characterization of reactive intermediates can be performed also by pulse radiolysis, a field that has been recently reviewed by Fujita et al.[106]

In a flash photolysis experiments, the transient spectrum recorded after the occurrence of the electron transfer from the WOC to PS^+ (i.e., after the recovery of the bleach when using $Ru(bpy)_3^{2+}$ as the PS) can be diagnostic for the formation of an oxidized species of the catalyst. This was the case for the $[Ru^{II}(NPM)(H_2O)(pic)_2]^{2+}$ (NPM = 4-tert-butyl-2,6-di-(1',8'-naphtyrid-2'-yl)-pyridine, pic = 4-picoline) WOC reported by Thummel and Fujita and described above,[78] where the ΔOD of the transient spectrum obtained after a proton coupled ET to $Ru(bpy)_3^{3+}$ revealed a positive ΔOD centered at 450 nm and a negative ΔOD centered at 610 nm, diagnostic for the one-electron oxidized form of the catalyst, $[Ru^{III}(NPM)(OH)(pic)_2]^{2+}$. Similarly, the electron transfer to photogenerated Ru(III) from the vanadium-based WOC $V_6O_7(OCH_3)_{12}^-$ reported by Campagna and coworkers[73] was followed not only through the recovery of the Ru(III)-related bleaching at 450 nm, but also *via* the formation of the featuring inter-valence charge-transfer (IVCT) transition at 405 nm ascribable to the $V_5^{(IV)}V^{(V)}O_7(OCH_3)_{12}$ one-electron oxidized WOC species.

Recently a very appealing approach for the characterization of Co_3O_4 nanoparticles intermediates, has been proposed by Frei and coworkers,[107] by exploiting time-resolved Fourier-transform infrared spectroscopy. In particular, upon photoirradiation of a $Ru(bpy)_3^{2+}/S_2O_8^{2-}$ aqueous suspension (pH 8) in the presence of 4-nm sized Co_3O_4 nanoparticles, the rising of two absorption peaks at 1013 and 840 cm^{-1} was attributed to a three-electron oxidized Co(III)OO superoxide intermediate and to a one-electron oxidized Co(IV)=O intermediate, respectively.[107] The different kinetic behavior of the two features suggests that the two intermediates originate from different surface sites. Indeed, the Co(III)OO superoxide intermediate was proposed to form at *fast* sites, wherein an adjacent Co(III)-OH moiety helps in stabilizing the superoxide species, that needs a further hole accumulation before oxygen evolution (Figure 8A). Conversely, the Co(IV)=O intermediate is formed by one-electron oxidation coupled to proton removal of a Co(III)-OH group at *slow* sites, characterized by the absence of an adjacent Co(III)-OH group. In this case, the Co(IV)=O group is proposed to undergo a water nucleophilic attack, coupled to proton removal, forming a Co(II)OOH hydroperoxide (Figure 8B).

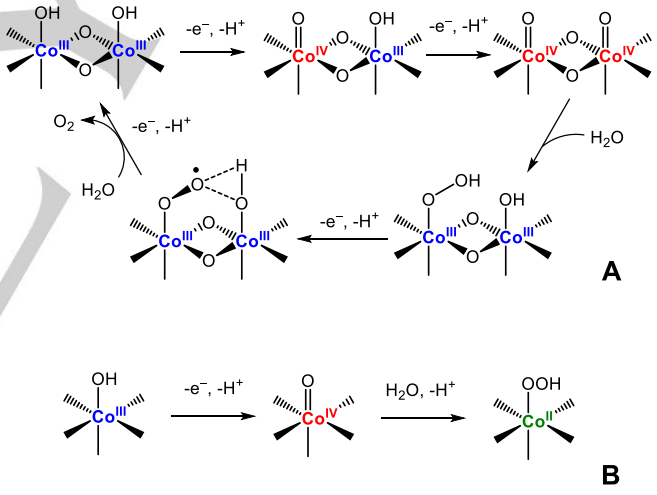

Figure 8. Proposed water oxidation catalytic mechanism by Co_3O_4 at A) fast surface sites and B) slow surface sites. Adapted from reference [107] with permission from Springer Nature.

Of course, intermediates with enough stability and lifetime can be photochemically generated with conventional methods and characterized with classical spectroscopy. Electron paramagnetic resonance (EPR) spectroscopy provides a pertinent case. By irradiation of a $Ru(bpy)_3^{2+}/S_2O_8^{2-}$ solution, in the presence of an iridium(III) complex carrying a di-carbene ligand as the WOC $([IrClCp^*(di\text{-}NHC)]^+$, with Cp* = pentamethylcyclopentadienyl and di-NHC = 1,1'-dimethyl-3,3'-ethylenediimidazole-2,2'-diylidene), an Ir-centered rhombic EPR signal arises, with *g* values = 2.4, 2.2 and 1.85.[108] This is

consistent with an Ir(IV) intermediate, characterized by a low-spin S=1/2 state,[109] likely involved in the photoinduced oxygen evolution cycle observed for this class of compounds.[108] A similar EPR signal (*g* values= 2.57, 2.09 and 1.83), diagnostic for an Ir(IV) intermediate formation was observed to originate upon photoirradiation of phosphorous porphyrin sensitized SnO_2 photoelectrode with a surface anchored Ir(III)Cp*Cl complex bearing a phenylpyridine based ligand.[110] Similar Ir(IV) photogenerated intermediates have been shown to form in covalent dyads with perylene bisimide photosensitizers.[111] EPR spectroscopy was employed also to identify a photogenerated intermediate form of the tetracobalt(III) cubane species described above. In particular, irradiation of a $Ru(bpy)_3^{2+}/S_2O_8^{2-}$ solution in the presence of the initially diamagnetic cubane (all cobalt centers in oxidation state III), induces the rising of a signal with axial line shape ($g_\perp$ = 2.33 and $g_\parallel$ = 2.07).[88] This is ascribed to the one-electron oxidized form of the cubane (known also as "cubium"),[112] characterized by a S = ½ and a formal $Co(III)_3Co(IV)$-oxo core, although the spin character is equally distributed among the four metal centers.[113,114] This evidence complements the kinetic information obtained by flash photolysis, and discussed in paragraph 3, on electron transfer from cubane to Ru(III). Although the "cubium" is not itself fast in reacting with water,[115] it quantitatively generates oxygen in the presence of OH^- either in alkaline aqueous solution or in organic solvents.[112,116] The loss of an acetate bridging ligand and the consequent opening of the coordination sphere of the cobalt centers seem pivotal for the oxygenic activity.[88] It is also worth mentioning that such intermediate was proposed as a molecular model of a Co(IV) active site of the Co-Pi heterogeneous catalyst.[113]

6. Conclusion and perspectives

In this microreview, we have aimed at presenting mechanistic insights related to light driven catalysis for water oxidation in EA/PS/WOC sacrificial cycles, trying to highlight the critical steps that may compromise the oxygenic performance. It is worth considering that the nature of the EA/PS/WOC sacrificial cycles is intrinsically different than the condition occurring in a dye-sensitized photoanode embedding a WOC. Therefore, caution should be taken in evaluating and transferring the information obtained from sacrificial cycles into the design of a photoanode. In table 3, we highlight the main differences to be considered between such systems.

First of all, photogeneration of PS^+ in a sacrificial cycle occurs through oxidative quenching by the EA (eq. 3), typically through bimolecular routes. For an efficient photoreaction triplet PS are thus required. Under diffusional control, even operating at high EA concentration, the timescale of PS^+ generation stands in the ns timescale. Conversely, in a dye-sensitized photoanode PS^+ generation occurs through *PS injection into the conduction band (CB) of the semiconductor, a process that can occur within hundreds fs.[117] This guarantees efficient injection also from singlet excited states, as has been demonstrated with recent reports employing subporphyrins[118] or bodipy[119] PS in photoelectrodes for water oxidation purposes. Electron injection from *PS can be also promoted by applying a positive bias to the semiconductor.

Table 3. Overview of the events occurring in photochemical water oxidation in EA/PS/WOC cycles or in a dye-sensitized photoanode embedding the WOC.

Event	EA/PS/WOC sacrificial cycle	PS/WOC dye-sensitized photoanode
Photogeneration of PS^+	Bimolecular; may occur in ns at high [EA]. Triplet *PS are needed.	May occur in hundreds fs. Singlet *PS are also suitable.
Hole scavenging	Bimolecular; μs – ms timescale	Unimolecular; ps-ns timescale
Unproductive/ productive *PS quenching by the WOC	Relevant only in case of PS/WOC association; ps-ns timescale	Highly relevant, dependent on PS-to-WOC ratio; ps-ns timescale

Concerning electron transfer from the WOC to PS^+ (hole scavenging), this is also expected to be accelerated in a photoelectrode, since it shifts from a bimolecular event in the EA/PS/WOC system (μs-ms timescale, see paragraph 3) to unimolecular ones, expected in ps-ns timescale. Nonetheless, the investigation of the hole scavenging process in the EA/PS/WOC system may reveal if significant activation barriers are associated to the WOC activation (as in the case of IrO_x, where slow ET to photogenerated Ru(III) oxidant occurs both in the sacrificial system[49] and at a photoanode[81,120]), or if external additives may enhance the electron transfer rate (as in the case of Co_3O_4 nanoparticles, where a base from the buffer enhances the rate of a proton coupled electron transfer to Ru(III) oxidant).[92] Other associated information from the ET in the EA/PS/WOC system deal with the number of ET from the WOC in a fixed timescale (typically ca 100 ms), and in the ET kinetic analysis of active intermediates of the WOC.[57]

As discussed in paragraph 4, quenching of *PS by the WOC (eq. 23) is detrimental towards the photoactivated oxygen evolution cycle. Although this event may be limited in EA/PS/WOC systems, either by lowering the WOC concentration or by limiting WOC/PS association,[70] this may become a serious issue in a dye-sensitized photoanode embedding the WOC. One relevant case is the Ru_4POM acting as a very efficient WOC in photoactivated cycles with $Ru(bpy)_3^{2+}/S_2O_8^{2-}$,[84] but displaying low performance in Ru polypyridine sensitized photoelectrodes.[69],[121] Ru_4POM was indeed shown to oxidatively quench the $*Ru(bpy)_3^{2+}$ when associated in ion pairs. In this sense, playing accurately with the PS-to-WOC ratio on the photoanode as well as on the anchoring groups and motif of both PS and WOC on the semiconducting surface may actually improve the efficiency.[122],[123] Also, a promising strategy to overcome this issue could be the employment of PS that favour the productive, reductive quenching by the WOC (eq. 24) rather than the unproductive oxidative quenching (eq. 23). This implies the use of PS being strong electron acceptors in the excited

state, such as the tetranuclear ruthenium dendrimer[104] or perylene bisiimides chromophores.[124,125],[126],[127]

Acknowledgments

We thank Prof. Franco Scandola (University of Ferrara), Prof. Marcella Bonchio (University of Padova) and Prof. Sebastiano Campagna (University of Messina) for many fruitful and inspiring discussions on the topics presented in this microreview. AS thanks the university of Padova and the department of chemical sciences for funding (Project PHOETRY, artificial photooxygenase for light assisted selective organic reactivity, P-DiSC #10BIRD2018-UNIPD).

Keywords

Electron transfer; intermediates; photocatalysis; reaction mechanisms; water oxidation

References

[1] S. Berardi, S. Drouet, L. Francàs, C. Gimbert-Suriñach, M. Guttentag, C. Richmond, T. Stoll, A. Llobet, *Chem. Soc. Rev.* **2014**, *43*, 7501–7519.

[2] H. Dau, E. Fujita, L. Sun, *ChemSusChem* **2017**, *10*, 4228–4235.

[3] A. Le Goff, V. Artero, B. Jousselme, P. D. Tran, N. Guillet, R. Métayé, A. Fihri, S. Palacin, M. Fontecave, *Science (80-.).* **2009**, *326*, 1384–1387.

[4] D. Strmcnik, P. P. Lopes, B. Genorio, V. R. Stamenkovic, N. M. Markovic, *Nano Energy* **2016**, *29*, 29–36.

[5] P. C. K. Vesborg, B. Seger, I. Chorkendorff, *J. Phys. Chem. Lett.* **2015**, *6*, 951–957.

[6] A. R. Zeradjanin, J. P. Grote, G. Polymeros, K. J. J. Mayrhofer, *Electroanalysis* **2016**, *28*, 2256–2269.

[7] R. Francke, B. Schille, M. Roemelt, *Chem. Rev.* **2018**, *118*, 4631–4701.

[8] H. Rao, L. C. Schmidt, J. Bonin, M. Robert, *Nature* **2017**, *548*, 74–77.

[9] P. Gao, S. Li, X. Bu, S. Dang, Z. Liu, H. Wang, L. Zhong, M. Qiu, C. Yang, J. Cai, W. Wei and Y. Sun *Nat. Chem.* **2017**, 9, 1019–1024.

[10] M. D. Kärkäs, B. Åkermark, *Dalt. Trans.* **2016**, *45*, 14421–14461.

[11] J. D. Blakemore, R. H. Crabtree, G. W. Brudvig, *Chem. Rev.* **2015**, *115*, 12974–13005.

[12] M. D. Kärkäs, O. Verho, E. V Johnston, B. Åkermark, *Chem. Rev.* **2014**, *114*, 11863–12001.

[13] X. Sala, S. Maji, R. Bofill, J. García-Antón, L. Escriche, A. Llobet, *Acc. Chem. Res.* **2014**, *47*, 504–516.

[14] J. Li, R. Güttinger, R. Moré, F. Song, W. Wan, G. R. Patzke, *Chem. Soc. Rev.* **2017**, *46*, 6124–6147.

[15] A. R. Parent, R. H. Crabtree, G. W. Brudvig, *Chem. Soc. Rev.* **2013**, *42*, 2247–2252.

[16] L. Duan, F. Bozoglian, S. Mandal, B. Stewart, T. Privalov, A. Llobet, L. Sun, *Nat. Chem.* **2012**, *4*, 418–423.

[17] A. Sartorel, P. Miró, E. Salvadori, S. Romain, M. Carraro, G. Scorrano, M. Di Valentin, A. Llobet, C. Bo, M. Bonchio, *J. Am. Chem. Soc.* **2009**, *131*, 16051–16053.

[18] J. L. Cape, W. F. Siems, J. K. Hurst, *Inorg. Chem.* **2009**, *48*, 8729–8735.

[19] J. A. Gilbert, D. S. Eggleston, W. R. Murphy, D. A. Geselowitz, S. W. Gersten, D. J. Hodgson, T. J. Meyer, *J. Am. Chem. Soc.* **1985**, *107*, 3855–3864.

[20] S. Romain, F. Bozoglian, X. Sala, A. Llobet, *J. Am. Chem. Soc.* **2009**, *131*, 2768–2769.

[21] X. Sala, M. Z. Ertem, L. Vigara, T. K. Todorova, W. Chen, R. C. Rocha, F. Aquilante, C. J. Cramer, L. Gagliardi, A. Llobet, *Angew. Chemie - Int. Ed.* **2010**, *49*, 7745–7747; *Angew. Chem.* **2010**, *122*, 7911–7913.

[22] K. J. Lee, N. Elgrishi, B. Kandemir, J. L. Dempsey, *Nat. Rev. Chem.* **2017**, *1*, article number 0039.

[23] J. Bonin, A. Maurin, M. Robert, *Coord. Chem. Rev.* **2017**, *334*, 184–198.

[24] C. Costentin, S. Drouet, M. Robert, J. M. Savéant, *J. Am. Chem. Soc.* **2012**, *134*, 11235–11242.

[25] C. Costentin, M. Robert, J. M. Savéant, *Acc. Chem. Res.* **2015**, *48*, 2996–3006.

[26] M. Okamura, M. Kondo, R. Kuga, Y. Kurashige, T. Yanai, S. Hayami, V. K. K. Praneeth, M. Yoshida, K. Yoneda, S. Kawata, et al., *Nature* **2016**, *530*, 465–468.

[27] Z. Chen, J. J. Concepcion, H. Luo, J. F. Hull, A. Paul, T. J. Meyer, *J. Am. Chem. Soc.* **2010**, *132*, 17670–17673.

[28] A. Prevedello, I. Bazzan, N. Dalle Carbonare, A. Giuliani, S. Bhardwaj, C. Africh, C. Cepek, R. Argazzi, M. Bonchio, S. Caramori, et al., *Chem. - An Asian J.* **2016**, *11*, 1281–1287.

[29] D. Wang, J. T. Groves, *Proc. Natl. Acad. Sci.* **2013**, *110*, 15579–15584.

[30] N. Song, J. J. Concepcion, R. A. Binstead, J. A. Rudd, A. K. Vannucci, C. J. Dares, M. K. Coggins, T. J. Meyer, *Proc. Natl. Acad. Sci.* **2015**, *112*, 4935–4940.

[31] T. Shinagawa, A. T. Garcia-Esparza, K. Takanabe, *Sci. Rep.* **2015**, *5*, 1–21.

[32] J. R. McKone, N. S. Lewis, H. B. Gray, *Chem. Mater.* **2014**, *26*, 407–414.

[33] F. Puntoriero, A. Sartorel, M. Orlandi, G. La Ganga, S. Serroni, M. Bonchio, F. Scandola, S. Campagna, *Coord. Chem. Rev.* **2011**, *255*, 2594–2601.

[34] A. Sartorel, M. Bonchio, S. Campagna, F. Scandola, *Chem. Soc. Rev.* **2013**, *42*, 2262–2280.

[35] T. Ishizuka, S. Ohkawa, H. Ochiai, M. Hashimoto, K. Ohkubo, H. Kotani, M. Sadakane, S. Fukuzumi, T. Kojima, *Green Chem.* **2018**, *20*, 1975–1980.

[36] S. Fukuzumi, T. Kojima, Y. M. Lee, W. Nam, *Coord. Chem. Rev.* **2017**, *333*, 44–56.

[37] S. Fukuzumi, T. Kishi, H. Kotani, Y.-M. Lee, W. Nam, *Nat. Chem.* **2011**, *3*, 38–41.

[38] D. R. Weinberg, C. J. Gagliardi, J. F. Hull, C. F. Murphy, C. A. Kent,

B. C. Westlake, A. Paul, D. H. Ess, D. G. McCafferty, T. J. Meyer, *Chem. Rev.* **2012**, *112*, 4016–4093.
[39] J. J. Warren, J. M. Mayer, *Biochemistry* **2015**, *54*, 1863–1878.
[40] S. Hammes-Schiffer, *J. Am. Chem. Soc.* **2015**, *137*, 8860–8871.
[41] F. Liu, J. J. Concepcion, J. W. Jurss, T. Cardolaccia, J. L. Templeton, T. J. Meyer, *Inorg. Chem.* **2008**, *47*, 1727–1752.
[42] B. H. Solis, S. Hammes-Schiffer, *Inorg. Chem.* **2014**, *53*, 6427–6443.
[43] S. Bensaid, C. Ottone Melis, S. Hernández, M. Armandi, S. Esposito, G. Saracco, B. Bonelli, *Chem. Eng. J.* **2017**, *311*, 143–152.
[44] M. K. Brennaman, R. J. Dillon, L. Alibabaei, M. K. Gish, C. J. Dares, D. L. Ashford, R. L. House, G. J. Meyer, J. M. Papanikolas, T. J. Meyer, *J. Am. Chem. Soc.* **2016**, *138*, 13085–13102.
[45] F. Puntoriero, S. Serroni, G. La Ganga, A. Santoro, M. Galletta, F. Nastasi, E. La Mazza, A. M. Cancelliere, S. Campagna, *Eur. J. Inorg. Chem.* **2018**, 3887–3899.
[46] A. Harriman, G. Porter, P. Walters, *J. Chem. Soc., Farad. Trans. 1* **1983**, *79*, 1335–1350.
[47] R. Memming, *J. Electrochem. Soc.* **1969**, *116*, 785.
[48] D. M. Stanbury, *Adv. Inorg. Chem.* **1989**, *33*, 69–138.
[49] N. D. Morris, M. Suzuki, T. E. Mallouk, *J. Phys. Chem. A* **2004**, *108*, 9115–9119.
[50] P. K. Ghosh, B. S. Brunschwig, M. Chou, C. Creutz, N. Sutin, *J. Am. Chem. Soc.* **1984**, *106*, 4772–4783.
[51] A. Juris, V. Balzani, F. Barigelletti, S. Campagna, P. Belser, A. von Zelewsky, *Coord. Chem. Rev.* **1988**, *84*, 85–277.
[52] H. S. White, W. G. Becker, A. J. Bard, *J. Phys. Chem.* **1984**, *88*, 1840–1846.
[53] A. Lewandowska-Andralojc, D. E. Polyansky, *J. Phys. Chem. A* **2013**, *117*, 10311–10319.
[54] F. Bolletta, M. Maestri, L. Moggi, V. Balzani, *J. Phys. Chem.* **1974**, *78*, 1374–1377.
[55] F. Bolletta, A. Juris, M. Maestri, D. Sandrini, *Inorganica Chim. Acta* **1980**, *44*, L175-L176.
[56] S. Berardi, L. Francàs, S. Neudeck, S. Maji, J. Benet-Buchholz, F. Meyer, A. Llobet, *ChemSusChem* **2015**, *8*, 3688–3696.
[57] L. Francàs, R. Matheu, E. Pastor, A. Reynal, S. Berardi, X. Sala, A. Llobet, J. R. Durrant, *ACS Catal.* **2017**, *7*, 5142–5150.
[58] G. S. Nahor, P. Neta, P. Hambright, A. N. Thompson, A. Harriman, *J. Phys. Chem.* **1989**, *93*, 6181–6187.
[59] Y. S. Nam, A. P. Magyar, D. Lee, J. W. Kim, D. S. Yun, H. Park, T. S. Pollom, D. A. Weitz, A. M. Belcher, *Nat. Nanotechnol.* **2010**, *5*, 340–344.
[60] K. Kalyanasundaram, M. Graetzel, *Curr. Opin. Biotechnol.* **2010**, *21*, 298–310.
[61] K. Kalyanasundaram, *Coord. Chem. Rev.* **1982**, *46*, 159–244.
[62] M. Natali, E. Deponti, D. Vilona, A. Sartorel, M. Bonchio, F. Scandola, *Eur. J. Inorg. Chem.* **2015**, *2015*, 3467–3477.
[63] H.-C. Chen, D. G. H. Hetterscheid, R. M. Williams, J. I. van der Vlugt, J. N. H. Reek, A. M. Brouwer, *Energy Environ. Sci.* **2015**, *8*, 975–982.
[64] J. Van Houten, R. J. Watts, *J. Am. Chem. Soc.* **1976**, *98*, 4853–4858.
[65] K. Kalyanasundaram, M. Neumannspallart, *J. Phys. Chem.* **1982**, *86*, 5163–5169.
[66] A. Harriman, G. Porter, P. Walters, *J. Chem. Soc., Faraday Trans.* **1981**, *2*, 2373–2383.
[67] E. M. Kober, B. P. Sullivan, W. J. Dressick, J. V. Caspar, T. J. Meyer, *J. Am. Chem. Soc.* **1980**, *102*, 7383–7385.
[68] I. Bazzan, A. Volpe, A. Dolbecq, M. Natali, A. Sartorel, P. Mialane, M. Bonchio, *Catal. Today* **2017**, *290*, 39–50.
[69] M. Orlandi, R. Argazzi, A. Sartorel, M. Carraro, G. Scorrano, M. Bonchio, F. Scandola, *Chem. Commun.* **2010**, *46*, 3152–3154.
[70] M. Natali, M. Orlandi, S. Berardi, S. Campagna, M. Bonchio, A. Sartorel, F. Scandola, *Inorg. Chem.* **2012**, *51*, 7324–7331.
[71] M. Natali, I. Bazzan, S. Goberna-Ferrón, R. Al-Oweini, M. Ibrahim, B. S. Bassil, H. Dau, F. Scandola, J. R. Galán-Mascarós, U. Kortz, et al., *Green Chem.* **2017**, *19*, 2416–2426.
[72] R. Al-Oweini, A. Sartorel, B. S. Bassil, M. Natali, S. Berardi, F. Scandola, U. Kortz, M. Bonchio, *Angew. Chemie - Int. Ed.* **2014**, *53*, 11182–11185; *Angew. Chem.* **2014**, *126*, 11364–11367.
[73] M. P. Santoni, G. La Ganga, V. Mollica Nardo, M. Natali, F. Puntoriero, F. Scandola, S. Campagna, *J. Am. Chem. Soc.* **2014**, *136*, 8189–8192.
[74] G. La Ganga, F. Puntoriero, S. Campagna, I. Bazzan, S. Berardi, M. Bonchio, A. Sartorel, M. Natali, F. Scandola, *Faraday Discuss.* **2012**, *155*, 177–190.
[75] S. Berardi, G. La Ganga, M. Natali, I. Bazzan, F. Puntoriero, A. Sartorel, F. Scandola, S. Campagna, M. Bonchio, *J. Am. Chem. Soc.* **2012**, *134*, 11104–11107.
[76] G. La Ganga, V. M. Nardo, M. Cordaro, M. Natali, S. Vitale, A. Licciardello, F. Nastasi, S. Campagna, *Dalt. Trans.* **2014**, *43*, 14926–14930.
[77] E. Pizzolato, M. Natali, B. Posocco, A. Montellano López, I. Bazzan, M. Di Valentin, P. Galloni, V. Conte, M. Bonchio, F. Scandola, et al., *Chem. Commun.* **2013**, *49*, 9941.
[78] A. Lewandowska-Andralojc, D. E. Polyansky, R. Zong, R. P. Thummel, E. Fujita, *Phys. Chem. Chem. Phys.* **2013**, *15*, 14058–14068.
[79] L. Wang, M. Mirmohades, A. Brown, L. Duan, F. Li, Q. Daniel, R. Lomoth, L. Sun, L. Hammarström, *Inorg. Chem.* **2015**, *54*, 2742–2751.
[80] M. Hara, C. C. Waraksa, J. T. Lean, B. A. Lewis, T. E. Mallouk, *J. Phys. Chem. A* **2000**, *104*, 5275–5280.
[81] W. J. Youngblood, S. A. Lee, Y. Kobayashi, E. A. Hernandez-pagan, P. G. Hoertz, T. A. Moore, A. L. Moore, D. Gust, T. E. Mallouk, D. P. Cell, **2009**, 926–927.
[82] W. J. Youngblood, S.-H. A. Lee, K. Maeda, T. E. Mallouk, *Acc. Chem. Res.* **2009**, *42*, 1966–1973.
[83] A. Agiral, H. Sen Soo, H. Frei, *Chem. Mater.* **2013**, *25*, 2264–2273.
[84] Y. V. Geletii, Z. Huang, Y. Hou, D. G. Musaev, T. Lian, C. L. Hill, *J. Am. Chem. Soc.* **2009**, *131*, 7522–7523.
[85] J. Yano, V. Yachandra, *Chem. Rev.* **2014**, *114*, 4175–4205.
[86] N. Cox, M. Retegan, F. Neese, D. A. Pantazis, A. Boussac, W. Lubitz, *Science (80-.).* **2014**, *345*, 804–808.
[87] V. Krewald, M. Retegan, N. Cox, J. Messinger, W. Lubitz, S. DeBeer, F. Neese, D. A. Pantazis, *Chem. Sci.* **2015**, *6*, 1676–1695.
[88] A. Genoni, G. La Ganga, A. Volpe, F. Puntoriero, M. Di Valentin, M. Bonchio, M. Natali, A. Sartorel, *Faraday Discuss.* **2015**, *185*, 121–

141.
[89] M. W. Kanan, D. G. Nocera, *Science (80-.).* **2008**, *321*, 1072–1075.
[90] D. G. Nocera, *Acc. Chem. Res.* **2012**, *45*, 767–776.
[91] S. Berardi, G. La Ganga, M. Natali, I. Bazzan, F. Puntoriero, A. Sartorel, F. Scandola, S. Campagna, M. Bonchio, *J. Am. Chem. Soc.* **2012**, *134*, 11104–11107.
[92] G. A. Volpato, A. Bonetto, A. Marcomini, P. Mialane, M. Bonchio, M. Natali, A. Sartorel, *Sustain. Energy Fuels* **2018**, *2*, 1951–1956.
[93] A. M. Ullman, C. N. Brodsky, N. Li, S. L. Zheng, D. G. Nocera, *J. Am. Chem. Soc.* **2016**, *138*, 4229–4236.
[94] H. Sen Soo, A. Agiral, A. Bachmeier, H. Frei, *J. Am. Chem. Soc.* **2012**, *134*, 17104–17116.
[95] E. Edri, J. K. Cooper, I. D. Sharp, D. M. Guldi, H. Frei, *J. Am. Chem. Soc.* **2017**, *139*, 5458–5466.
[96] J. De Tovar, N. Romero, S. A. Denisov, R. Bofill, C. Gimbert-Suriñach, D. Ciuculescu-Pradines, S. Drouet, A. Llobet, P. Lecante, V. Colliere, et al., *Mater. Today Energy* **2018**, *9*, 506–515.
[97] L. Wang, D. L. Ashford, D. W. Thompson, T. J. Meyer, J. M. Papanikolas, *J. Phys. Chem. C* **2013**, *117*, 24250–24258.
[98] S. E. Bettis, K. Hanson, L. Wang, M. K. Gish, J. J. Concepcion, Z. Fang, T. J. Meyer, J. M. Papanikolas, *J. Phys. Chem. A* **2014**, *118*, 10301–10308.
[99] A. M. López, M. Natali, E. Pizzolato, C. Chiorboli, M. Bonchio, A. Sartorel, F. Scandola, *Phys. Chem. Chem. Phys.* **2014**, *16*, 12000–12007.
[100] S. Serroni, S. Campagna, F. Puntoriero, C. Di Pietro, N. D. McClenaghan, F. Loiseau, *Chem. Soc. Rev.* **2001**, *30*, 367–375.
[101] F. Puntoriero, F. Nastasi, M. Cavazzini, S. Quici, S. Campagna, *Coord. Chem. Rev.* **2007**, *251*, 536–545.
[102] F. Puntoriero, S. Serroni, G. La Ganga, A. Santoro, M. Galletta, F. Nastasi, E. La Mazza, A. M. Cancelliere, S. Campagna, *Eur. J. Inorg. Chem.* **2018**, 1–13.
[103] Designing Dendrimers*. Sebastiano Campagna, Paola Ceroni and Fausto Puntoriero editors*, John Wiley & Sons Inc publisher, Hoboken New Jersey, **2012**.
[104] M. Natali, F. Puntoriero, C. Chiorboli, G. La Ganga, A. Sartorel, M. Bonchio, S. Campagna, F. Scandola, *J. Phys. Chem. C* **2015**, *119*, 2371–2379.
[105] M. Burian, Z. Syrgiannis, G. La Ganga, F. Puntoriero, M. Natali, F. Scandola, S. Campagna, M. Prato, M. Bonchio, H. Amenitsch, A. Sartorel, *Inorganica Chim. Acta* **2017**, *454*, 171–175.
[106] D. C. Grills, D. E. Polyansky, E. Fujita, *ChemSusChem* **2017**, *10*, 4359–4373.
[107] M. Zhang, M. De Respinis, H. Frei, *Nat. Chem.* **2014**, *6*, 362–367.
[108] A. Volpe, A. Sartorel, C. Tubaro, L. Meneghini, M. Di Valentin, C. Graiff, M. Bonchio, *Eur. J. Inorg. Chem.* **2014**, 665–675.
[109] T. P. Brewster, J. D. Blakemore, N. D. Schley, C. D. Incarvito, N. Hazari, G. W. Brudvig, R. H. Crabtree, *Organometallics* **2011**, *30*, 965–973.
[110] P. K. Poddutoori, J. M. Thomsen, R. L. Milot, S. W. Sheehan, C. F. A. Negre, V. K. R. Garapati, C. A. Schmuttenmaer, V. S. Batista, G. W. Brudvig, A. Van Der Est, *J. Mater. Chem. A* **2015**, *3*, 3868–3879.
[111] M. T. Vagnini, A. L. Smeigh, J. D. Blakemore, S. W. Eaton, N. D. Schley, F. D'Souza, R. H. Crabtree, G. W. Brudvig, D. T. Co, M. R. Wasielewski, *Proc. Natl. Acad. Sci.* **2012**, *109*, 15651–15656.
[112] P. F. Smith, L. Hunt, A. B. Laursen, V. Sagar, S. Kaushik, K. U. D. Calvinho, G. Marotta, E. Mosconi, F. De Angelis, G. C. Dismukes, *J. Am. Chem. Soc.* **2015**, *137*, 15460–15468.
[113] J. G. McAlpin, Y. Surendranath, M. Dinca, T. a. Stich, S. a. Stoian, W. H. Casey, D. G. Nocera, R. D. Britt, M. Dincã, T. a. Stich, et al., *J. Am. Chem. Soc.* **2010**, *4*, 6882–6883.
[114] C. N. Brodsky, R. G. Hadt, D. Hayes, B. J. Reinhart, N. Li, L. X. Chen, D. G. Nocera, *Proc. Nat. Acad. Sci. U.S.A.* **2017**, *114*, 3855–3860.
[115] A. M. Ullman, Y. Liu, M. Huynh, D. K. Bediako, H. Wang, B. L. Anderson, D. C. Powers, J. J. Breen, H. D. Abruña, D. G. Nocera, *J. Am. Chem. Soc.* **2014**, *136*, 17681–17688.
[116] A. I. Nguyen, M. S. Ziegler, P. Oña-Burgos, M. Sturzbecher-Hohne, W. Kim, D. E. Bellone, T. D. Tilley, *J. Am. Chem. Soc.* **2015**, *137*, 12865–12872.
[117] T. A. Heimer, E. J. Heilweil, C. A. Bignozzi, G. J. Meyer, *J. Phys. Chem. A* **2000**, *104*, 4256–4262.
[118] M. Yamamoto, Y. Nishizawa, P. Chábera, F. Li, T. Pascher, V. Sundström, L. Sun, H. Imahori, *Chem. Commun.* **2016**, *52*, 13702–13705.
[119] O. Suryani, Y. Higashino, J. Y. Mulyana, M. Kaneko, T. Hoshi, K. Shigaki, Y. Kubo, *Chem. Commun.* **2017**, *53*, 6784–6787.
[120] J. R. Swierk, T. E. Mallouk, *Chem. Soc. Rev.* **2013**, *42*, 2357–2387.
[121] J. Fielden, J. M. Sumliner, N. Han, Y. V. Geletii, X. Xiang, D. G. Musaev, T. Lian, C. L. Hill, *Chem. Sci.* **2015**, *6*, 5531–5543.
[122] Y. Gao, L. Zhang, X. Ding, L. Sun, *Phys. Chem. Chem. Phys.* **2014**, *16*, 12008–12013.
[123] H. Y. Chen, S. Ardo, *Nat. Chem.* **2018**, *10*, 17–23.
[124] F. Ronconi, Z. Syrgiannis, A. Bonasera, M. Prato, R. Argazzi, S. Caramori, V. Cristino, C. A. Bignozzi, *J. Am. Chem. Soc.* **2015**, *137*, 4630–4633.
[125] J. T. Kirner, R. G. Finke, *J. Mater. Chem. A* **2017**, *5*, 19560–19592.
[126] F. Würthner, C. R. Saha-Möller, B. Fimmel, S. Ogi, P. Leowanawat, D. Schmidt, *Chem. Rev.* **2016**, *116*, 962–1052.
[127] M. Bonchio, Z. Syrgiannis, M. Burian, N. Marino, E. Pizzolato, K. Dirian, F. Rigodanza, G. A. Volpato, G. La Ganga, N. Demitri, S. Berardi, H. Amenitsch, D. M. Guldi, S. Caramori, C. A. Bignozzi, A. Sartorel, M. Prato, *Nat. Chem.* **2019**, in press, DOI 10.1038/s41557-018-0172-y.

10.1002/ejic.201801236

WILEY-VCH

Entry for the Table of Contents

MICROREVIEW

The mechanistic aspects of photoinduced water oxidation catalysis are discussed, including elemental steps, electron transfer rates, alternative pathways, catalyst intermediates identification. Perspectives are given for the transfer of such mechanistic information towards the design of dye-sensitized photoanodes embedding the catalyst.

Water oxidation photocatalysis

Mirco Natali, Francesco Nastasi, Fausto Puntoriero, Andrea Sartorel**

Page No. – Page No.

Mechanistic insights into light-activated catalysis for water oxidation